Supporting Information

Shengyang Guan,[†] Thomas Pickl,[†] Christian Jandl, Leon Schuchmann, Xiaoyu Zhou, Philipp J. Altmann and Alexander Pöthig*

Catalysis Research Center & Department of Chemistry, Technische Universität München, Ernst-Otto-Fischer-Str. 1, 85747 Garching bei München, Germany.

1. General Remarks

Chemicals were purchased from commercial suppliers and used without further purification if not stated otherwise. NMR spectra in solution were recorded on a Bruker Avance DPX 400 and a Bruker DRX 400 spectrometer at room temperature if not stated otherwise. Chemical shifts are given in parts per million (ppm) and scalar coupling constants ^{n}J are given in Hertz (Hz). the spectra were referenced to the residual solvent shift of the deuterated solvent as an internal standard (D_2O: ^{1}H NMR δ 4.79; MeCN-d_3: ^{1}H NMR δ 1.94, ^{13}C NMR δ 118.26; DMSO-d_6: ^{1}H NMR δ 2.50, ^{13}C NMR δ 39.52). ^{13}C NMR spectra in D_2O were referenced by addition of methanol as a standard. ESI-MS analyses were performed on a Thermo Scientific LCQ/Fleet spectrometer by Thermo Fisher Scientific. Elemental analyses were measured by the microanalytical laboratory at the Technical University of Munich using a HEKAtech Euro EA – CHNS combustion analyser. Emission spectra were measured on a Hamamatsu Absolute PL Quantum Yield C11347 spectrometer.

2. NMR Spectra of Compound 4

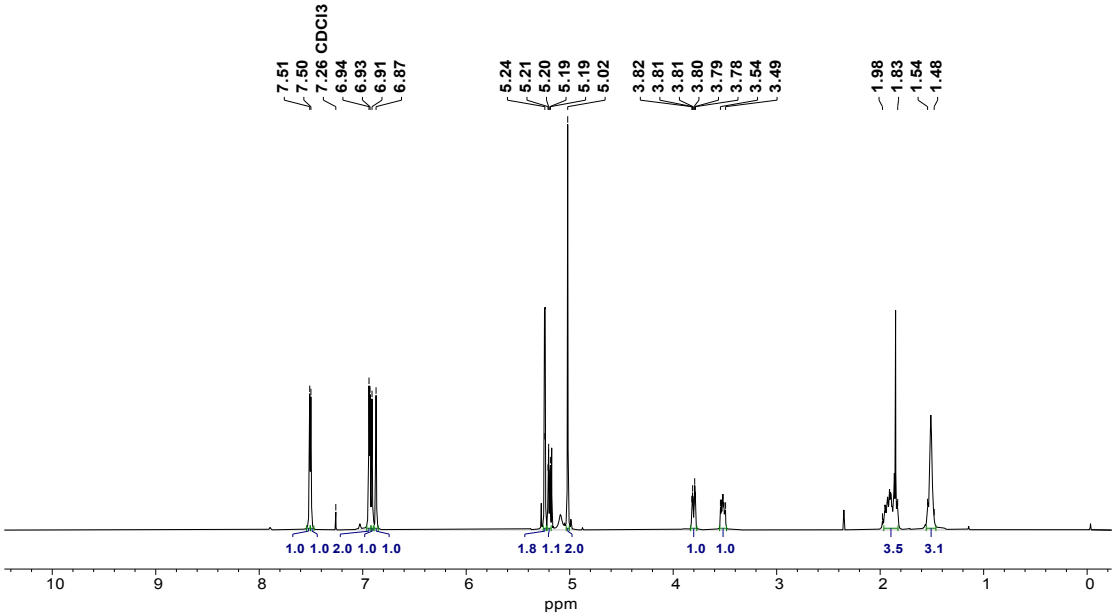

Figure S1. ^{1}H NMR spectrum of **3,5-bis((1*H*-imidazol-1-yl)methyl)-1-(tetrahydro-2*H*-pyran-2-yl)-1*H*-1,2,4-triazole, 4** in $CDCl_3$ at 400.13 MHz.

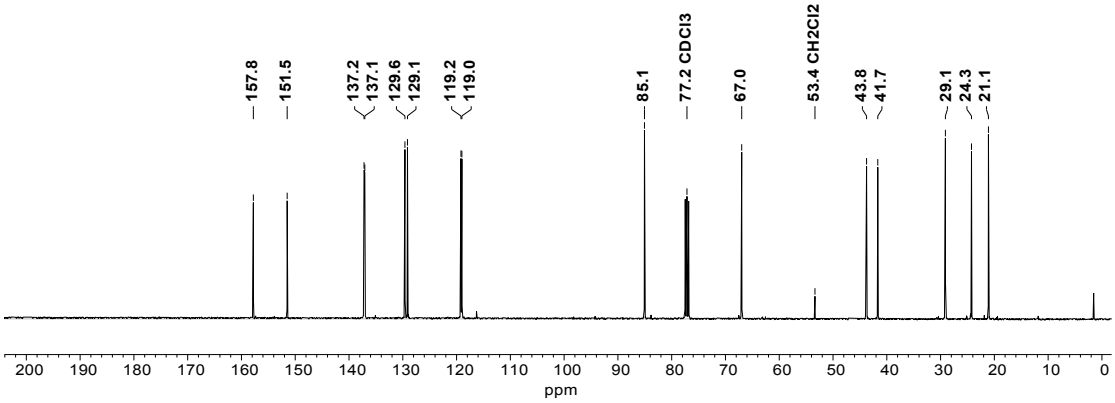

Figure S2. ^{13}C NMR spectrum of **3,5-bis((1*H*-imidazol-1-yl)methyl)-1-(tetrahydro-2*H*-pyran-2-yl)-1*H*-1,2,4-triazole, 4** in $CDCl_3$ at 100.62 MHz.

3. NMR Spectra of $H_6L^t(OTf)_4$

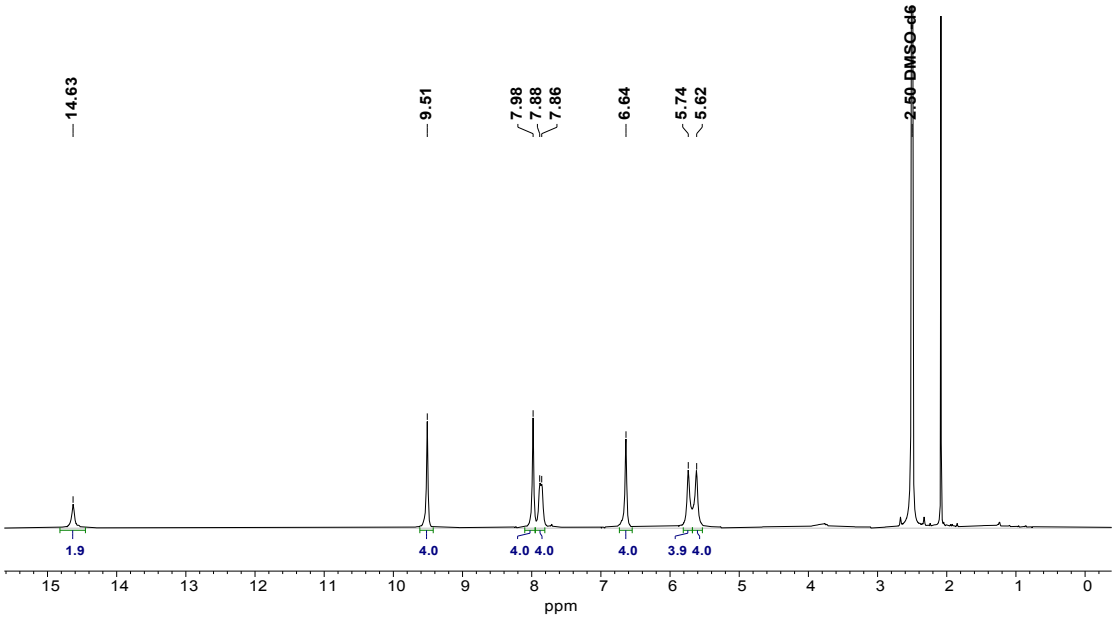

Figure S3. ^{1}H NMR spectrum of **$H_6L^t(OTf)_4$** in DMSO-d_6 at 400.13 MHz.

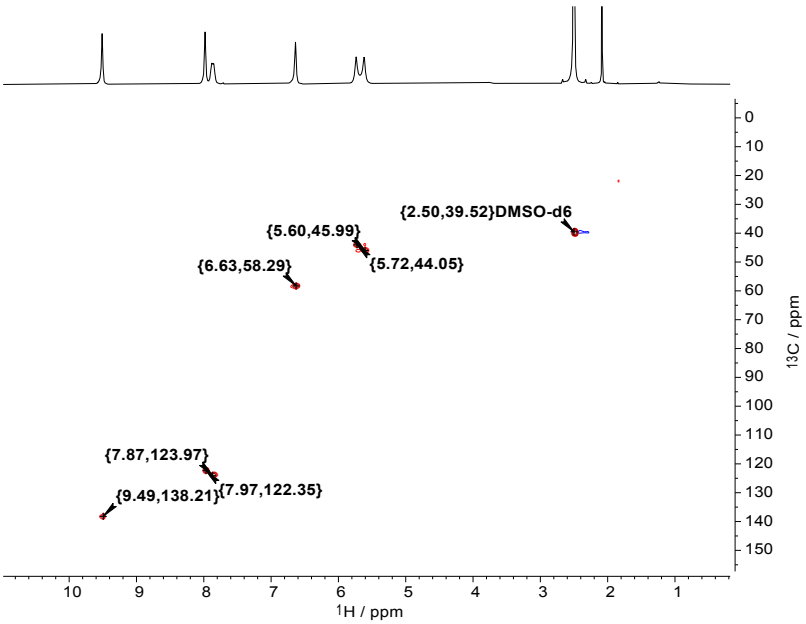

Figure S4. ^{1}H,^{13}C HSQC NMR spectrum of **$H_6L^t(OTf)_4$** in DMSO-d_6 at 400.13 MHz.

4. NMR Spectra of $[Ag_8L^t_2](OTf)_4$

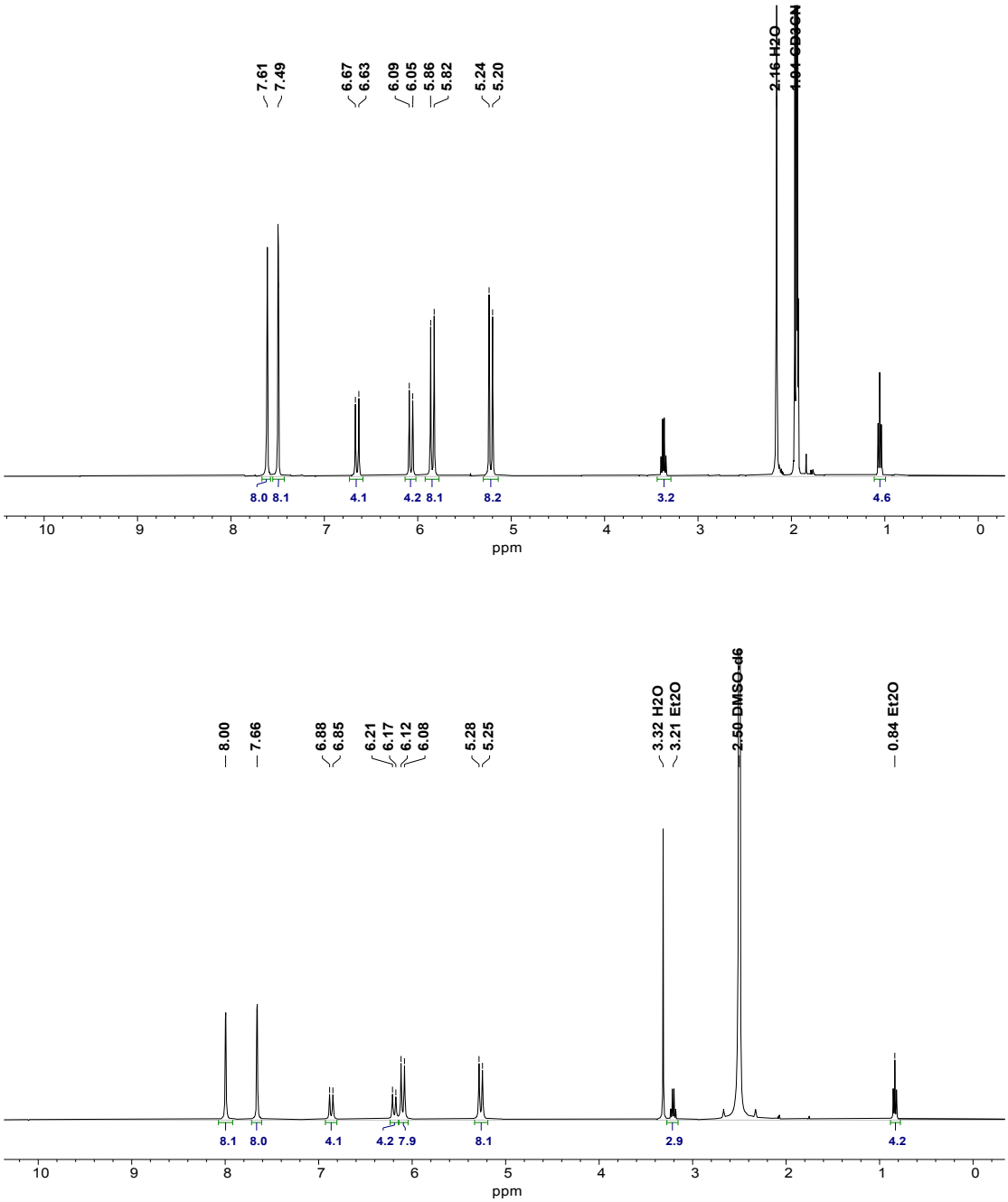

Figure S5. ^{1}H NMR spectra of **$[Ag_8L^t_2](OTf)_4$** in MeCN-d_3 (top) and DMSO-d_6 (bottom) at 400.13 MHz. One molecule of diethyl ether remains in the pore of the pillarplex.

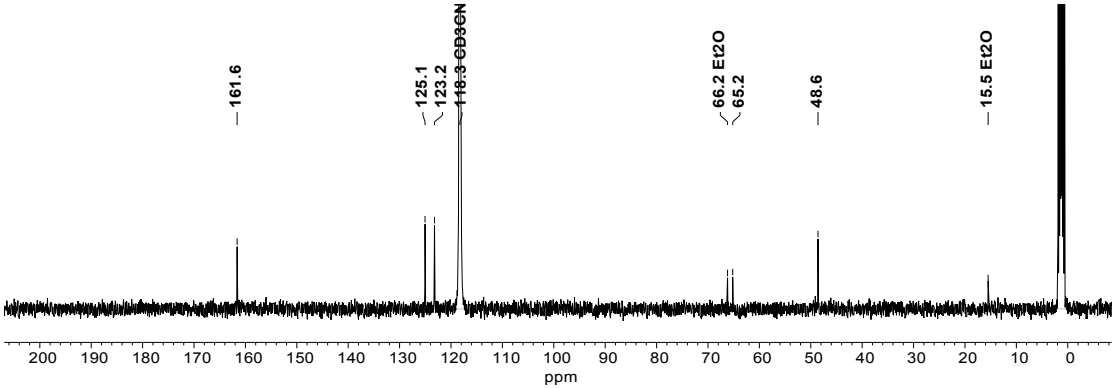

Figure S6. ^{13}C NMR spectrum of **[$Ag_8L^t_2$](OTf)$_4$** in MeCN-d_3 at 100.62 MHz.

5. NMR Spectra of $[Ag_8L^t_2](PF_6)_4$

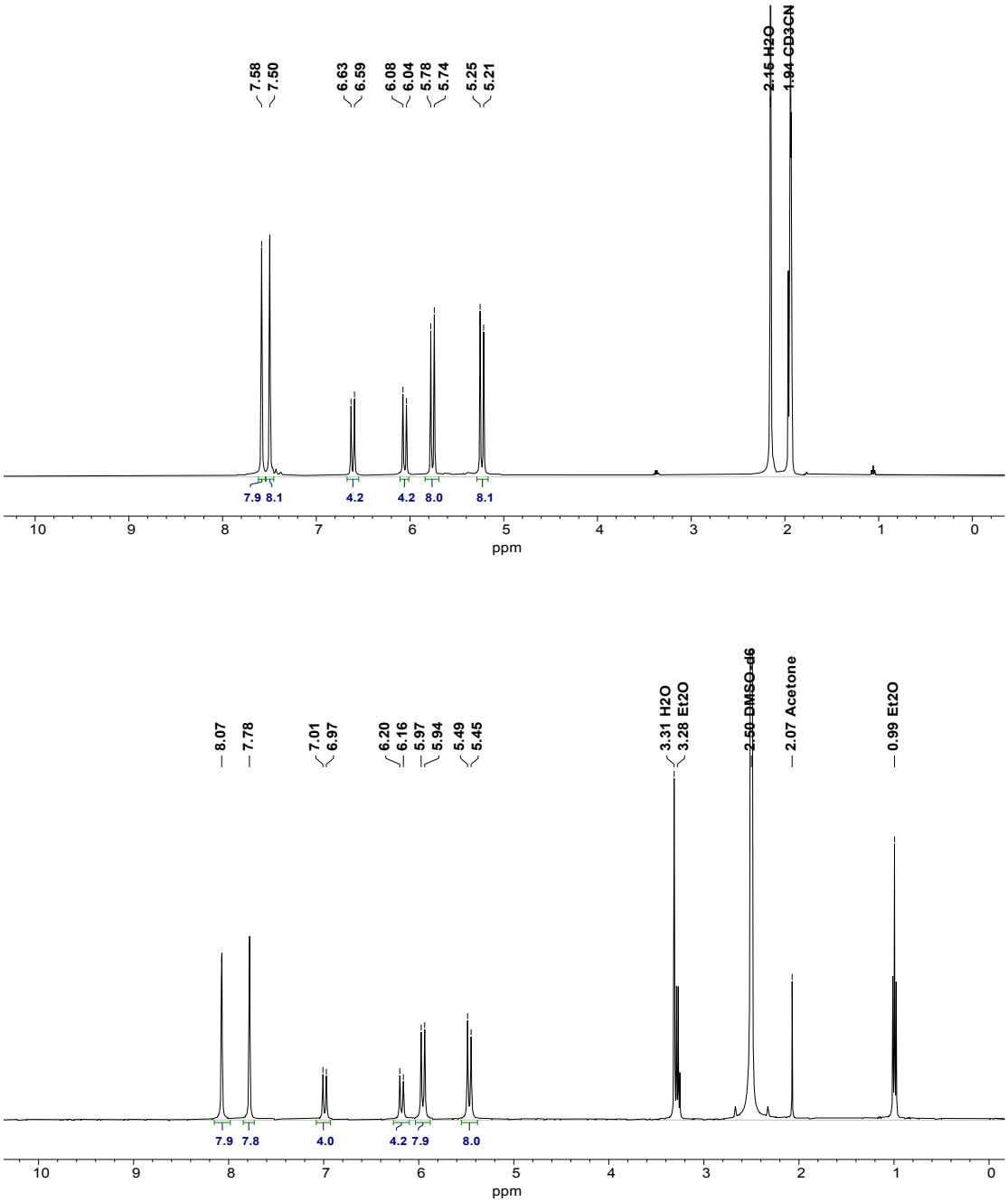

Figure S7. ^{1}H NMR spectra of $[Ag_8L^t_2](PF_6)_4$ in MeCN-d_3 (top) and DMSO-d_6 (bottom) at 400.13 MHz.

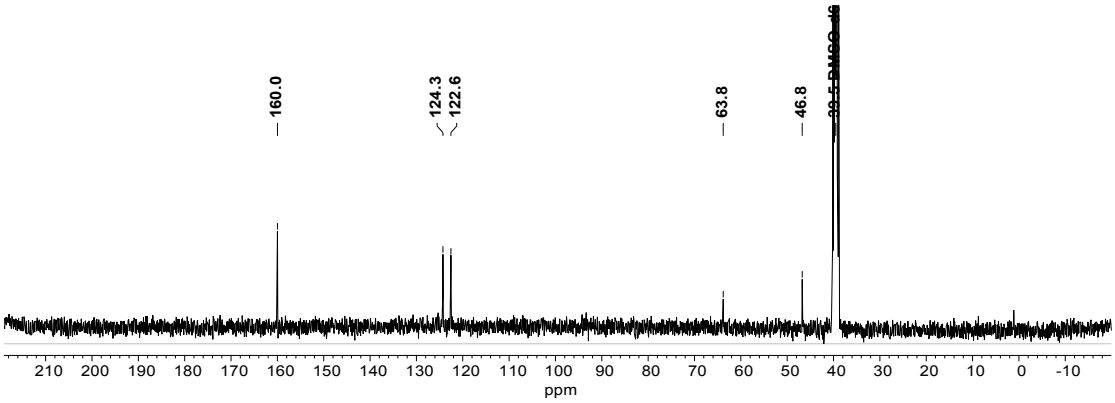

Figure S8. ^{13}C NMR spectrum of **[$Ag_8L^t_2$](PF_6)$_4$** in DMSO-d_6 at 100.62 MHz.

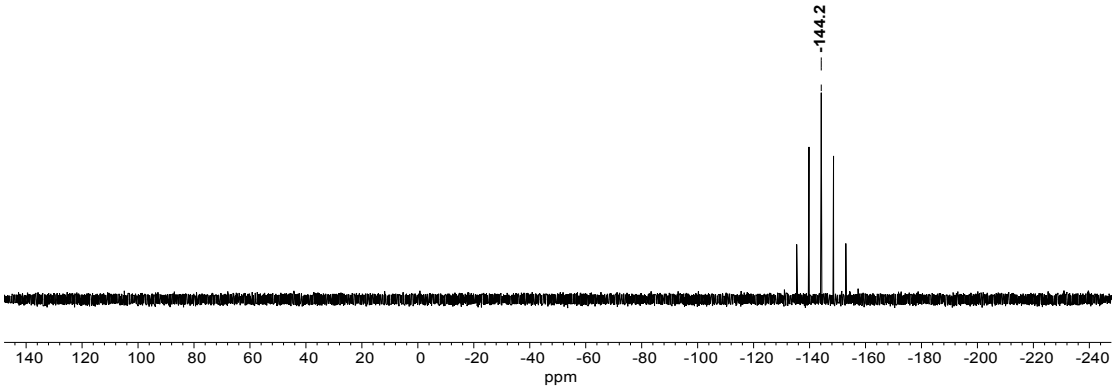

Figure S9. ^{31}P NMR spectrum of **[$Ag_8L^t_2$](PF_6)$_4$** in DMSO-d_6 at 161.97 MHz.

6. NMR Spectra of $[Au_8L^t_2](PF_6)_4$

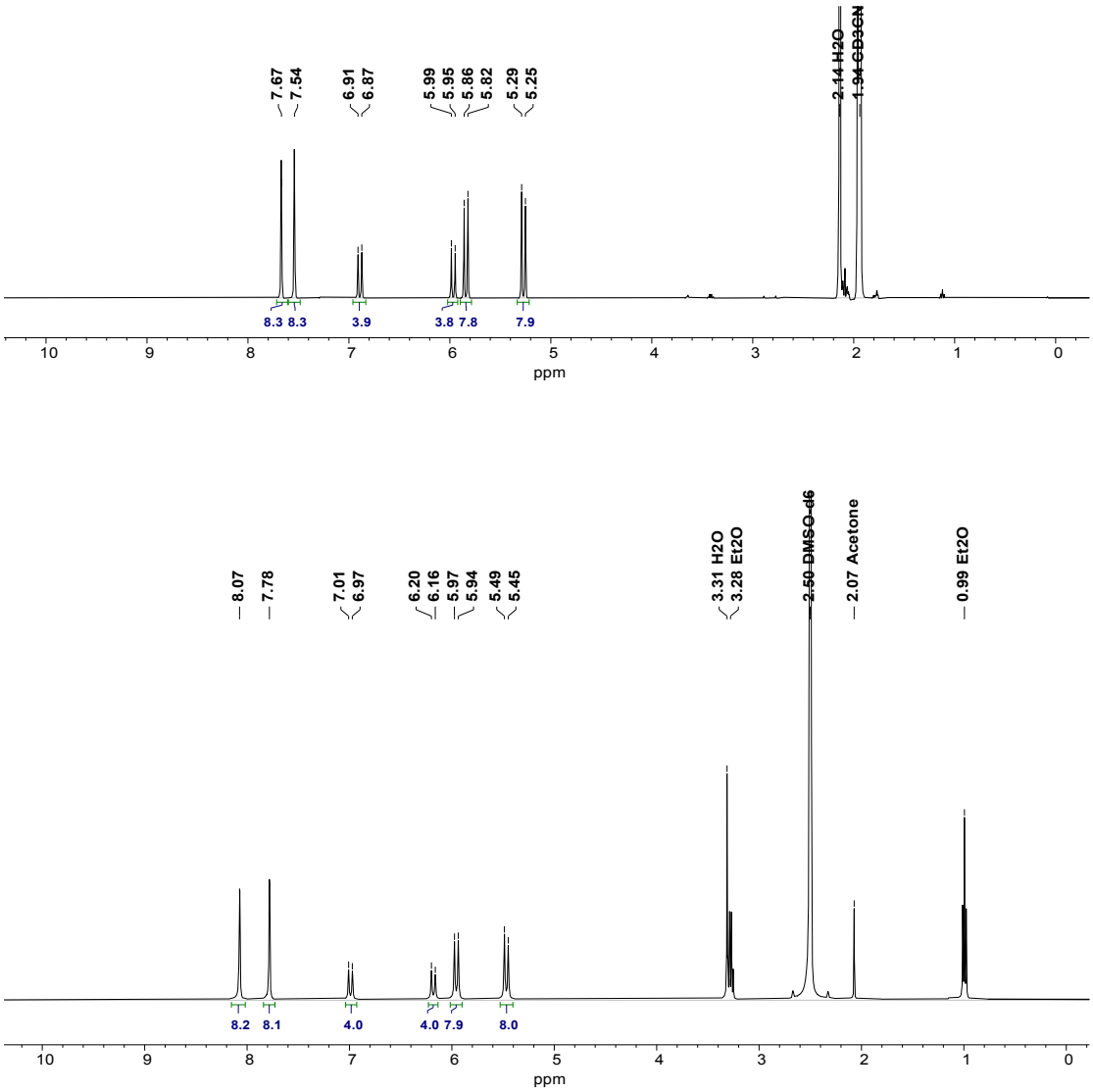

Figure S10. ^{1}H NMR spectra of $\mathbf{[Au_8L^t_2](PF_6)_4}$ in MeCN-d_3 (top) and DMSO-d_6 (bottom) at 400.13 MHz.

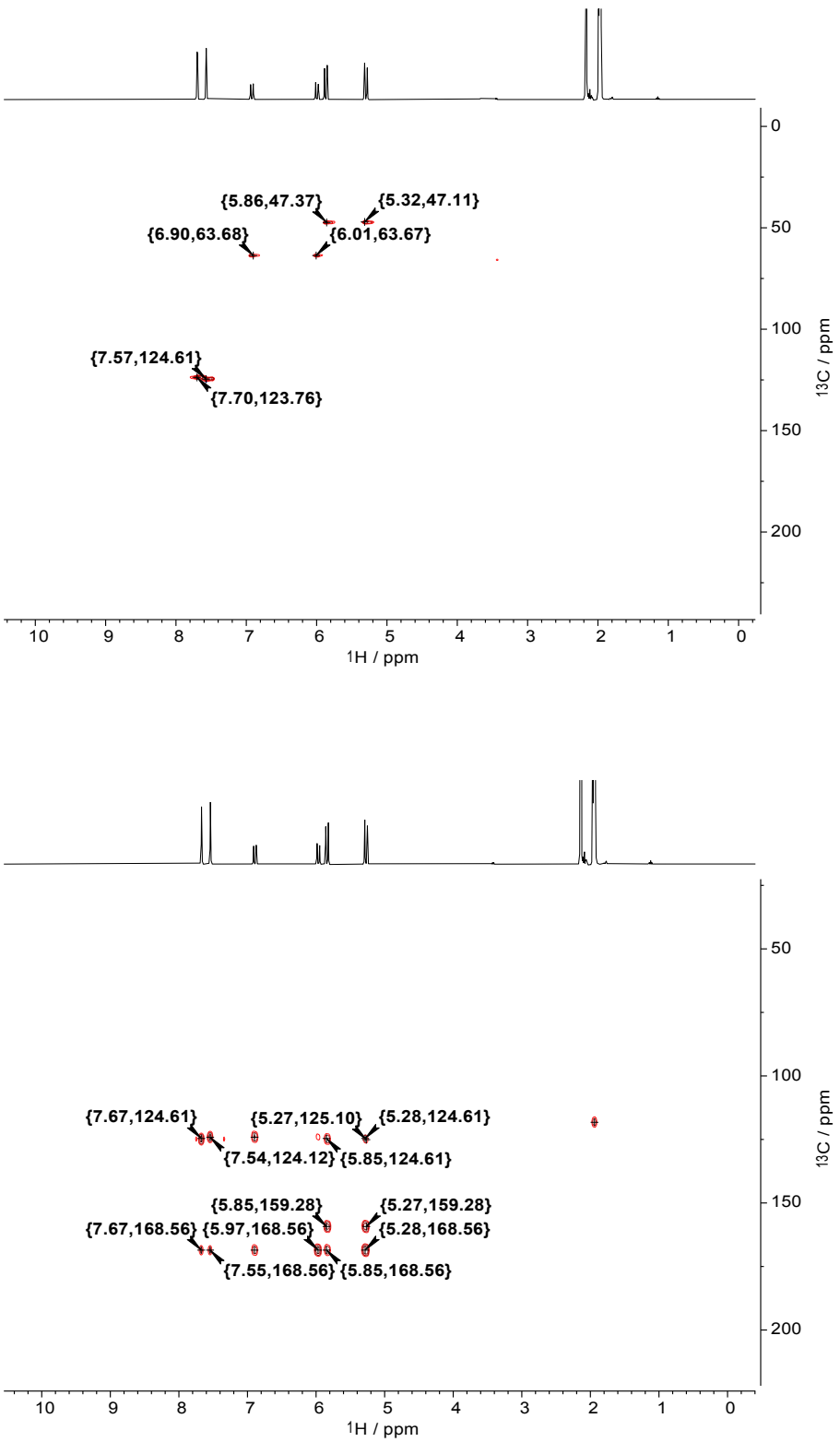

Figure S11. $^{1}H,^{13}C$ HSQC (top) and HMBC spectra (bottom) of **$[Au_8L^t_2](PF_6)_4$** in MeCN-d_3 at 400.13 MHz.

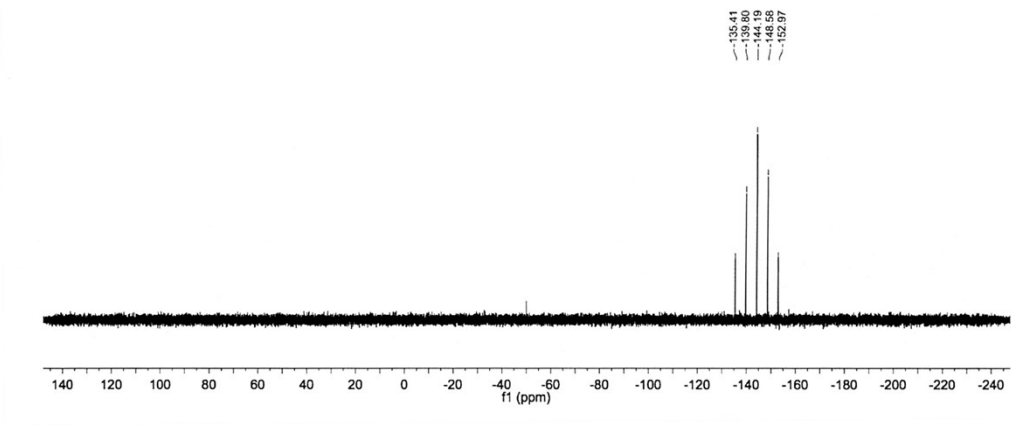

Figure S12. ^{31}P NMR spectrum of **[$Au_8L^t_2$](PF_6)$_4$** in DMSO-d_6 at 161.97 MHz.

7. ESI-MS Spectra

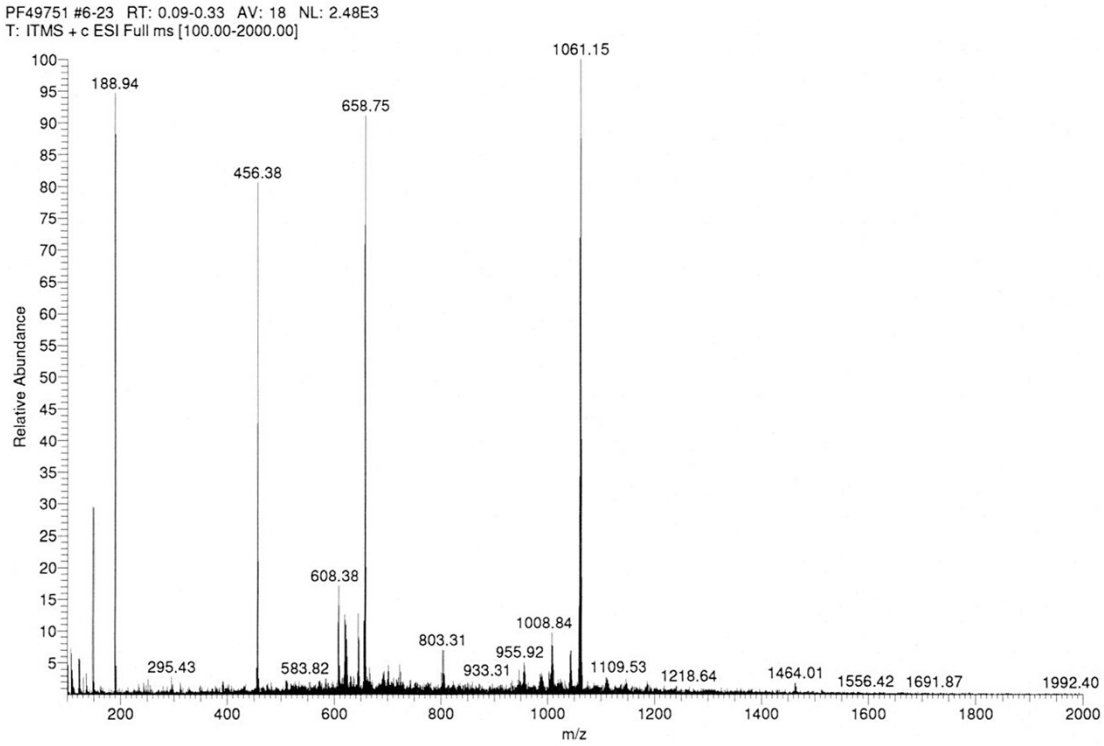

Figure S13. ESI-MS spectrum of compound **[$Ag_8L^t_2$](OTf)$_4$**.

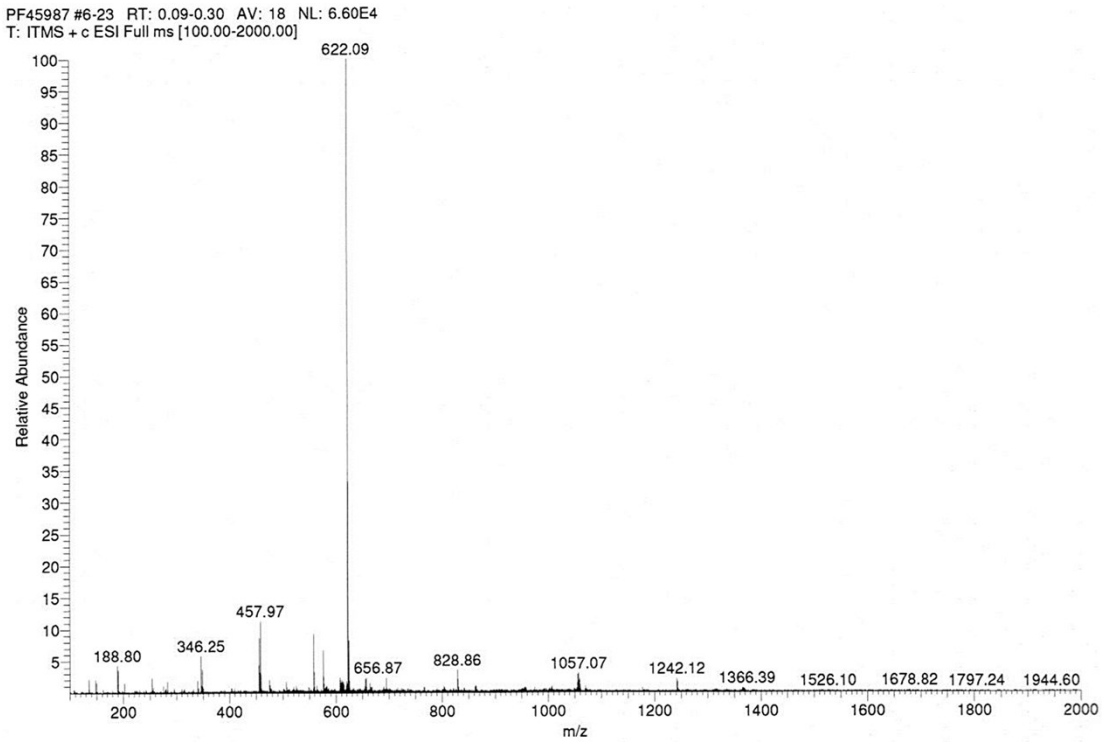

Figure S14. ESI-MS spectrum of compound **[$Ag_8L^t_2$](PF_6)$_4$**.

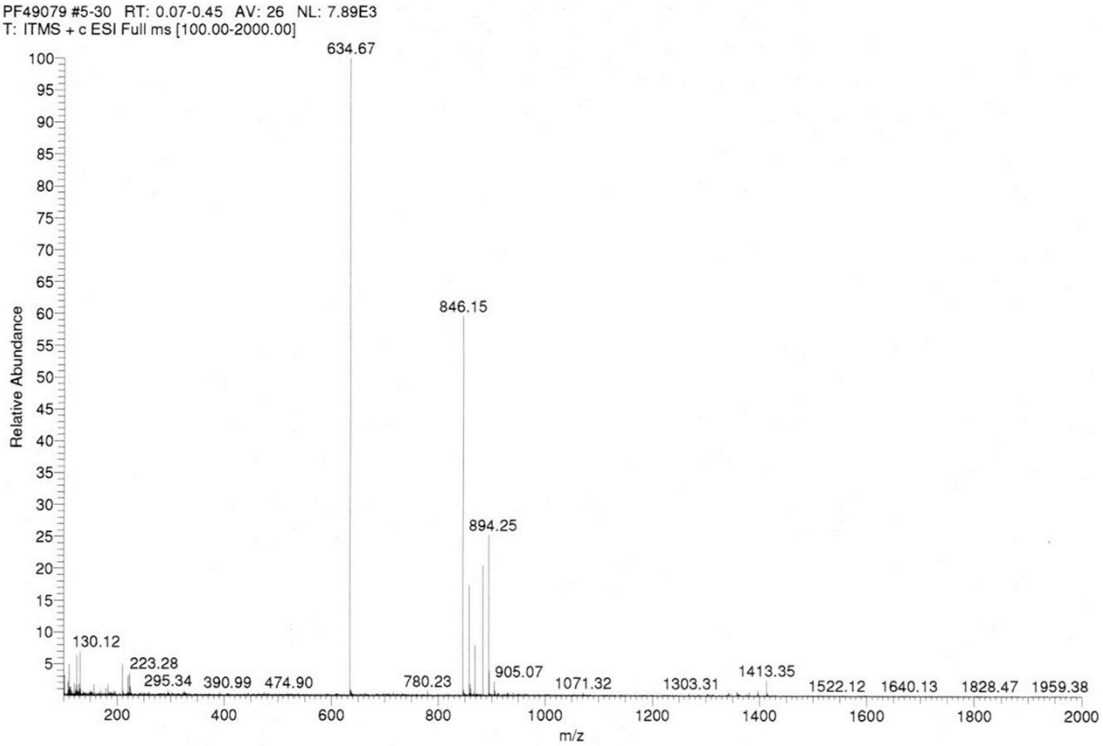

Figure S15. ESI-MS spectrum of compound **[$Au_8L^t_2$](PF_6)$_4$**.

8. Job-Plot Titrations

To determine the binding stoichiometry of 1,8-diaminooctane and $[Au_8L^t_2](PF_6)_4$, Job Plot titrations were performed in MeCN-d_3, followed by ^{1}H NMR spectroscopy.[1,2] Stock solutions (2.4 mM) of the gold complex $[Au_8L^t_2](PF_6)_4$ (host) and 1,8-diaminooctane (guest) were prepared. For each experiment, eleven samples were prepared with a different host–guest ratio so that the overall concentration ([host]+[guest]) for each sample was 1.2 mM.

Table S1. Data for the Job plot titration of $[Au_8L^t_2](PF_6)_4$ and 1,8-diaminooctane in MeCN-d_3.

No.	V host	V guest	[host]	[guest]	[guest]/([host]+[guest])	δ	Δδ	(Δδ)[guest]/([host]+[guest])
	(µL)	(µL)	(mM)	(mM)		(ppm)	(ppm)	
1	0	500	0	1.200	1	1.292	0	0
2	50	450	0.12	1.080	0.9	1.238	0.054	0.0486
3	100	400	0.24	0.960	0.8	1.179	0.113	0.0904
4	150	350	0.36	0.840	0.7	1.093	0.199	0.1393
5	200	300	0.48	0.720	0.6	0.975	0.317	0.1902
6	250	250	0.6	0.600	0.5	0.847	0.445	0.2225
7	300	200	0.72	0.480	0.4	0.782	0.51	0.204
8	350	150	0.84	0.360	0.3	0.858	0.434	0.1302
9	400	100	0.96	0.240	0.2	0.957	0.335	0.067
10	450	50	1.08	0.120	0.1	0.957	0.335	0.0335
11	500	0	1.2	0.000	0	0	1.292	0

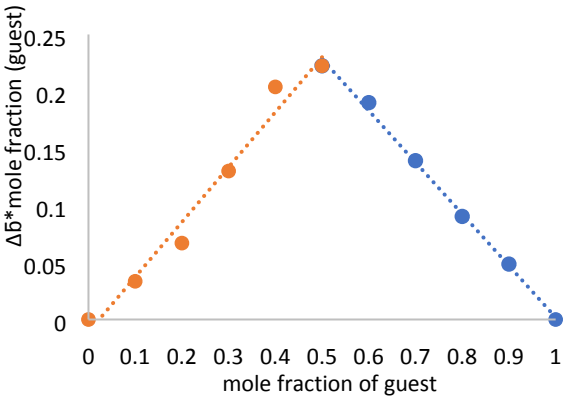

Figure S16. Job-plot of titration of **$[Au_8L^t_2](PF_6)_4$** against 1,8 diaminooctane in MeCN-d_3. The maximum was found at a mole fraction of the guest of 0.5, indicating a 1:1 stoichiometry of the interaction.

9. Determination of the Host–Guest Binding Constant by NMR Titration

Line fitting and determination of the dissociation constant K_d of the NMR titration data was performed using DynaFit[3] (nonlinear least-squares regression analysis). To a 1.425 mM solution of 1,8-diaminooctane (guest) in MeCN-d_3, was added the host **$[Au_8L^t_2](PF_6)_4$** in small aliquots. In this equilibrium binding experiment, the total concentration of the titrant changes due to the inevitable dilution. This was accounted for by using the keywords *plot titration* and *variable* (listing the names of two molecular species) in the *[data]* block of the DynaFit input file. The concentration-dependent shift of the NMR resonance of methylene proton H_A (directly attached to the amino group, *cf.* Figure 5) was used as the response. This is also in experimental agreement with in our previous study.[4]

c_0(guest) [M]	1,43E-03
c_0(host) [M]	2,85E-03

eq(host)	c(host) [mM]	c(guest) [mM]	$\delta(H_A)$ [ppm]
0,0	0	1,43	2,598
0,2	0,26	1,30	2,292
0,4	0,48	1,19	2,078
0,6	0,66	1,10	1,735
0,8	0,81	1,02	1,522
1,0	0,95	0,95	1,346
2,0	1,43	0,71	1,294
3,0	1,71	0,57	1,289

10. Solid-State Smission Spectrum of $[Au_8L^t_2](PF_6)_4$

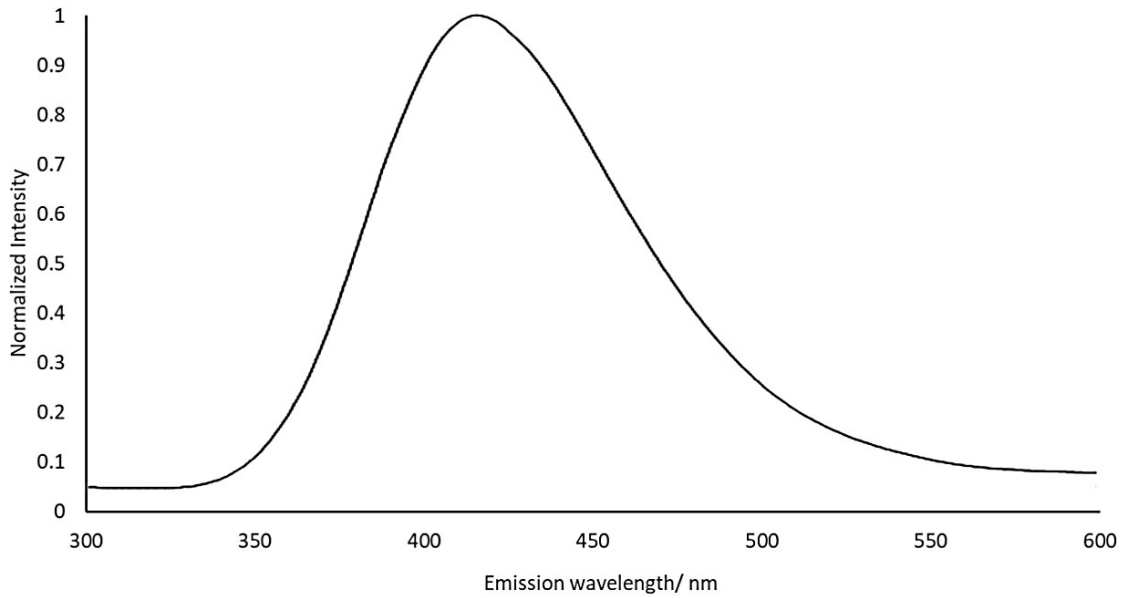

Figure S17. Emission spectrum of $\mathbf{[Au_8L^t_2](PF_6)_4}$ (solid state, λ_{ex} = 270 nm). We screened excitation wavelengths from 250 nm to 400 nm to find the highest emission intensity.

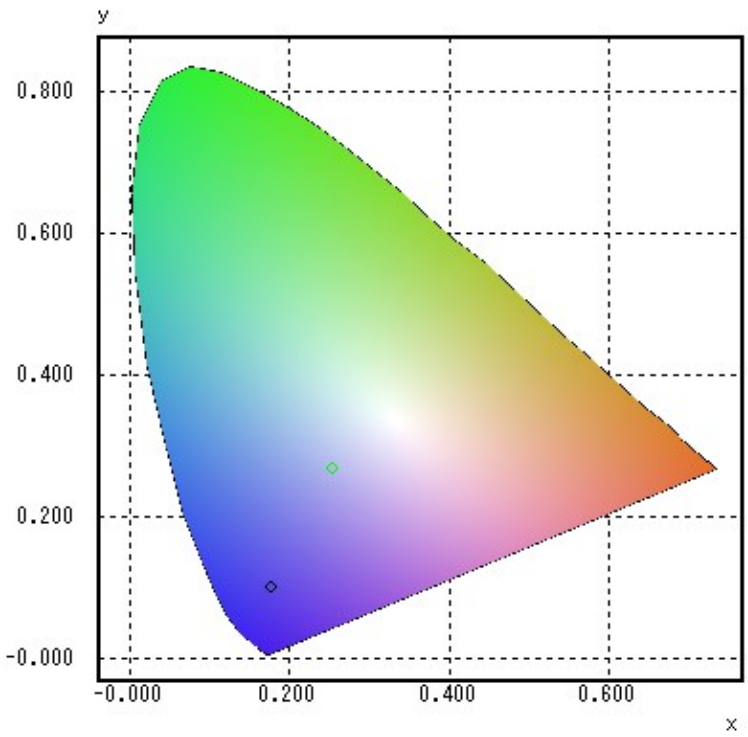

Figure S18. CIE color space chromaticity diagram with the emission of $\mathbf{[Au_8L^t_2](PF_6)_4}$ circled in green, excitation circled in black.

11. Computational Methods

All DFT calculations were performed with the ORCA 4.2.0 quantum chemistry package[5-7] using the Perdew–Burke–Ernzerhof (PBE) exchange-correlation functional[8] and the def2-TZVP triple-ξ valence basis set including one polarization function for H, C, N, and Au.[8] To account for relativistic effects, a full Stuttgart–Dresden effective core potential (def2-ECP)[9] for Au was employed. Tighter than normal SCF convergence criteria (TightSCF), finer than default grids (Grid4), and the 'resolution-of-identity' (RI-J) approximation with def2/J as an auxiliary basis set were employed as implemented in ORCA.[10] To account for dispersion interactions, Grimme's atom-pairwise dispersion correction (D3) with the Becke-Johnson damping scheme (BJ) was applied.[11,12] Geometries were optimised in the gas phase without any symmetry constraint. The total energy of the (fully and partially) optimised structures was found to depend on the distance defined by the outermost NHC backbone carbon atoms (NHC-Pyrazole-NHC or NHC-Triazole-NHC) which was constrained incrementally. A second-degree polynomial regression was used to accurately correlate the relative total energy ΔΔE (kJ/mol) of $\mathbf{[Au_8L^t_2]^{4+}}$ and $\mathbf{[Au_8L^{Me}_2]^{4+}}$ with the portal opening d_{calcd} (Å) of the complexes. The following functions were used to calculate the energies associated with selected portal openings:

$\mathbf{[Au_8L^t_2]^{4+}}$: $\Delta\Delta E(d_{calcd}) = 19{,}03\cdot(d_{calcd})^2 - 177{,}77\cdot(d_{calcd}) + 415{,}47$

$\mathbf{[Au_8L^{Me}_2]^{4+}}$: $\Delta\Delta E(d_{calcd}) = 20{,}77\cdot(d_{calcd})^2 - 229{,}94\cdot(d_{calcd}) + 636{,}98$

12. Crystallographic Details

Data were collected on a Bruker D8 Venture single crystal X-ray diffractometer equipped with a CMOS detector (Bruker Photon-100), a TXS rotating anode with MoK_{α} radiation (λ = 0.71073 Å) and a Helios optic using the APEX3 software package.[13] Measurements were performed on single crystals coated with perfluorinated ether. The crystals were fixed on top of a Kapton micro sampler and frozen under a stream of cold nitrogen. A matrix scan was used to determine the initial lattice parameters. Reflections were corrected for Lorentz and polarisation effects, scan speed, and background using SAINT.[14] Absorption corrections, including odd and even ordered spherical harmonics were performed using SADABS. [14] Space group assignments were based upon systematic absences, E statistics, and successful refinement of the structures. The structures were solved using SHELXT with the aid of successive difference Fourier maps, and were refined against all data using SHELXL in conjunction with SHELXLE.[15-17] Hydrogen atoms were calculated in ideal positions as follows: Methyl H atoms were refined as part of rigid rotating groups, with a C–H distance of 0.98 Å and $U_{iso}(H) = 1.5 \cdot U_{eq}(C)$. Non-methyl H atoms were placed in calculated positions and refined using a riding model, with methylene, aromatic, and other C–H distances of 0.99 Å, 0.95 Å and 1.00 Å, respectively, and $U_{iso}(H) = 1.2 \cdot U_{eq}(C)$. Non-hydrogen atoms were refined with anisotropic displacement parameters. Full-matrix least-squares refinements were carried out by minimizing $\Sigma w(F_o^2 - F_c^2)^2$ with the SHELXL weighting scheme.[15] Neutral atom scattering factors for all atoms and anomalous dispersion corrections for the non-hydrogen atoms were taken from *International Tables for Crystallography*.[18] The unit cell of **$[Ag_8L^t_2](OTf)_4$** contains 4 molecules of diethyl ether and 8 molecules of acetonitrile and the unit cell of **$[Au_8L^t_2](PF_6)_4$** contains 8 molecules of diethyl ether which were all treated as a diffuse contribution to the overall scattering without specific atom positions using the PLATON/SQUEEZE procedure.[19] Images of the crystal structures were generated with Mercury and PLATON.[20,21] CCDC 2077680 and 2077681 contains the supplementary crystallographic data for this paper. These data are provided free of charge by The Cambridge Crystallographic Data Centre.

[$Ag_8L^t_2$](OTf)$_4$ (CCDC 2077680)

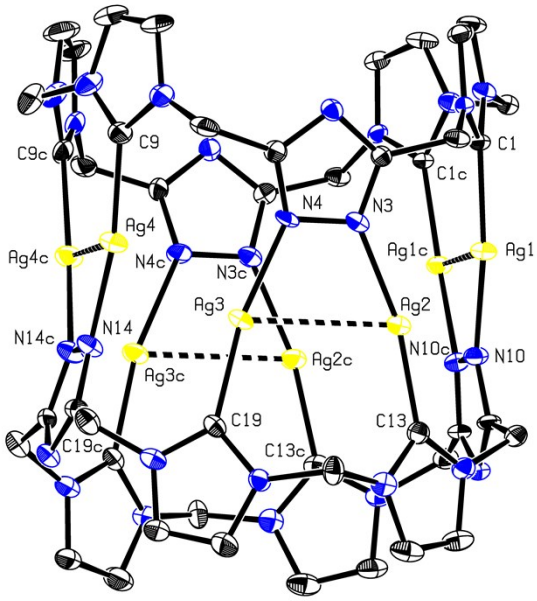

Figure S19. Crystal structure of **[$Ag_8L^t_2$](OTf)$_4$** cation, ADPs are given at 50% probability level.

Identification code	GuaSh17
Diffractometer operator	C. Jandl
scan speed	1-10 s per frame
2805 frames measured in 9 data sets	
phi-scans with delta_phi = 0.5	
omega-scans with delta_omega = 0.5	
Mode	shutterless mode
Crystal data	
$C_{22}H_{20}Ag_4N_{14}\cdot 2(CF_3O_3S)$	
M_r = 1210.14	D_x = 2.029 Mg m^{-3}
Orthorhombic, *Pnma*	Melting point: ? K
Hall symbol: -P 2ac 2n	Mo *K*α radiation, λ = 0.71073 Å
a = 19.357 (7) Å	Cell parameters from 6188 reflections
b = 21.269 (8) Å	θ = 2.4–26.3°
c = 19.244 (7) Å	μ = 2.14 mm^{-1}
V = 7923 (5) Å^3	*T* = 100 K
Z = 8	Fragment, colourless
F(000) = 4672	0.31 × 0.24 × 0.13 mm
Data collection	
Bruker D8 Venture diffractometer	7736 independent reflections
Radiation source: TXS rotating anode	7276 reflections with $I > 2\sigma(I)$
Helios optic monochromator	R_{int} = 0.051
Detector resolution: 16 pixels mm^{-1}	θ_{max} = 25.7°, θ_{min} = 2.3°

phi– and ω–rotation scans	h = −23 23
Absorption correction: multi-scan *SADABS* 2016/2, Bruker	k = −25 25
T_{min} = 0.654, T_{max} = 0.745	l = −23 23
82118 measured reflections	
Refinement	
Refinement on F^2	Secondary atom site location: difference Fourier map
Least-squares matrix: full	Hydrogen site location: inferred from neighbouring sites
$R[F^2 > 2\sigma(F^2)]$ = 0.055	H-atom parameters constrained
$wR(F^2)$ = 0.132	W = 1/[Σ²(*FO*²) + 148.9416*P*] WHERE *P* = (*FO*² + 2*FC*²)/3
S = 1.26	$(\Delta/\sigma)_{max}$ < 0.001
7736 reflections	$\Delta\rho_{max}$ = 1.22 e Å^{-3}
657 parameters	$\Delta\rho_{min}$ = −1.41 e Å^{-3}
792 restraints	Extinction correction: none
0 constraints	Extinction coefficient: -
Primary atom site location: iterative	

$[Au_8L^t_2](PF_6)_4$ (CCDC 2077681)

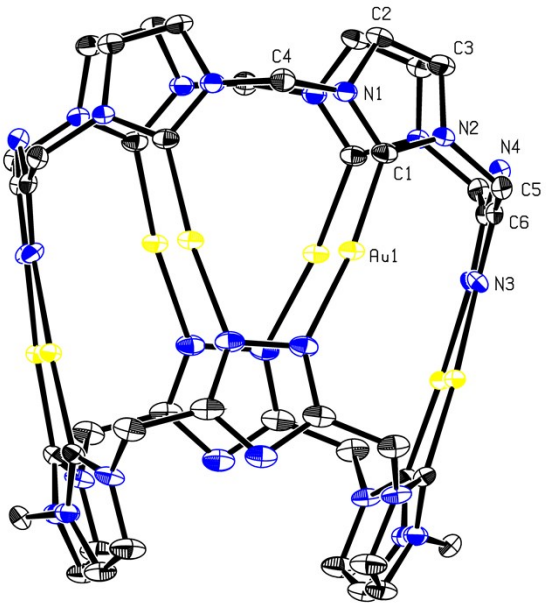

Figure S20. Crystal structure of **$[Au_8L^t_2](PF_6)_4$** cation, ADPs are given at 50% probability level.

Identification code	GuaSh11
Diffractometer operator	C. Jandl
scan speed	2-20 s per frame

1205 frames measured in 9 data sets	
phi-scans with delta_phi = 0.5	
omega-scans with delta_omega = 0.5	
Mode	shutterless mode
Crystal data	
$C_{44}H_{40}Au_8N_{28}\cdot4(F_6P)$	D_x = 2.590 Mg m^{-3}
M_r = 3116.68	Melting point: ? K
Tetragonal, *I*4/*mcm*	Mo *K*α radiation, λ = 0.71073 Å
Hall symbol: -I 4 2c	Cell parameters from 9902 reflections
a = 16.222 (4) Å	θ = 2.5–26.7°
c = 30.371 (8) Å	μ = 14.81 mm^{-1}
V = 7992 (4) Å^3	*T* = 103 K
Z = 4	Cube, colourless
F(000) = 5632	0.08 × 0.06 × 0.03 mm

Data collection	
Bruker D8 Venture diffractometer	2199 independent reflections
Radiation source: TXS rotating anode	1932 reflections with $I > 2\sigma(I)$
Helios optic monochromator	R_{int} = 0.031
Detector resolution: 16 pixels mm^{-1}	θ_{max} = 26.4°, θ_{min} = 2.5°
phi– and ω–rotation scans	*h* = −20 20
Absorption correction: multi-scan *SADABS* 2016/2, Bruker	*k* = −19 20
T_{min} = 0.643, T_{max} = 0.745	*l* = −37 37
35016 measured reflections	
Refinement	
Refinement on F^2	Secondary atom site location: difference Fourier map
Least-squares matrix: full	Hydrogen site location: inferred from neighbouring sites
$R[F^2 > 2\sigma(F^2)]$ = 0.020	H-atom parameters constrained
$wR(F^2)$ = 0.044	$W = 1/[\Sigma^2(FO^2) + (0.0052P)^2 + 115.086P]$ WHERE $P = (FO^2 + 2FC^2)/3$
S = 1.15	$(\Delta/\sigma)_{max}$ = 0.003
2199 reflections	$\Delta\rho_{max}$ = 0.95 e Å^{-3}
150 parameters	$\Delta\rho_{min}$ = −0.75 e Å^{-3}
0 restraints	Extinction correction: none

0 constraints	Extinction coefficient: -
Primary atom site location: iterative	

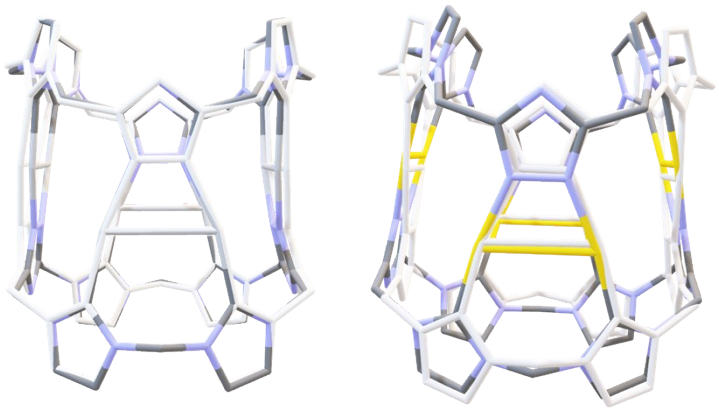

Figure S21. (Left) Overlay of pyrazolate silver pillarplex **[$Ag_8L^{Me}_2$]$^{4+}$** (atoms and bonds are bleached to white) and triazole based silver pillarplex **[$Ag_8L^t_2$] $^{4+}$** and (right) overlay of pyrazolate gold pillarplex **[$Au_8L^{Me}_2$]$^{4+}$** (atoms and bonds are bleached to white) and triazole based gold pillarplex **[$Au_8L^t_2$] $^{4+}$**.

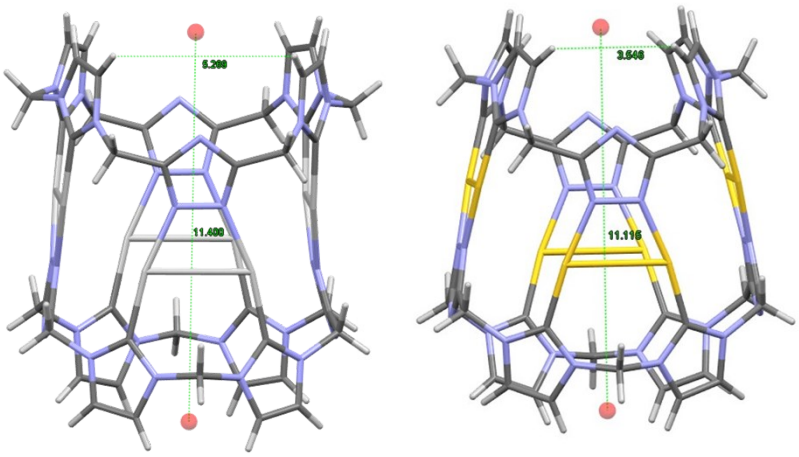

Figure S22. (Left) Calculation method for the height of the pillarplexes: distance between two centroids defined by all backbone NHC protons of each rim. (Right) Calculation method for the portal opening of the pillarplexes: averaged distance of the outermost backbone protons minus 2x covalence radius of hydrogen (0.31 Å).[22]

Table S1. Structural parameters of the Au^I-NHC moieties in **[$Au_8L^t_2$](PF_6)$_4$** and **[$Au_8L^{Me}_2$](PF_6)$_4$**

	[$Au_8L^t_2$](PF_6)$_4$	**[$Au_8L^{Me}_2$](PF_6)$_4$**
Au-N bond length / Å	2.040	2.055*
Au-C bond length / Å	1.986	1.968*
intramolecular Au···Au distance / Å	3.003	2.996*
C-Au-N angle / °	171.6	170.9*

*average value for distances and angles

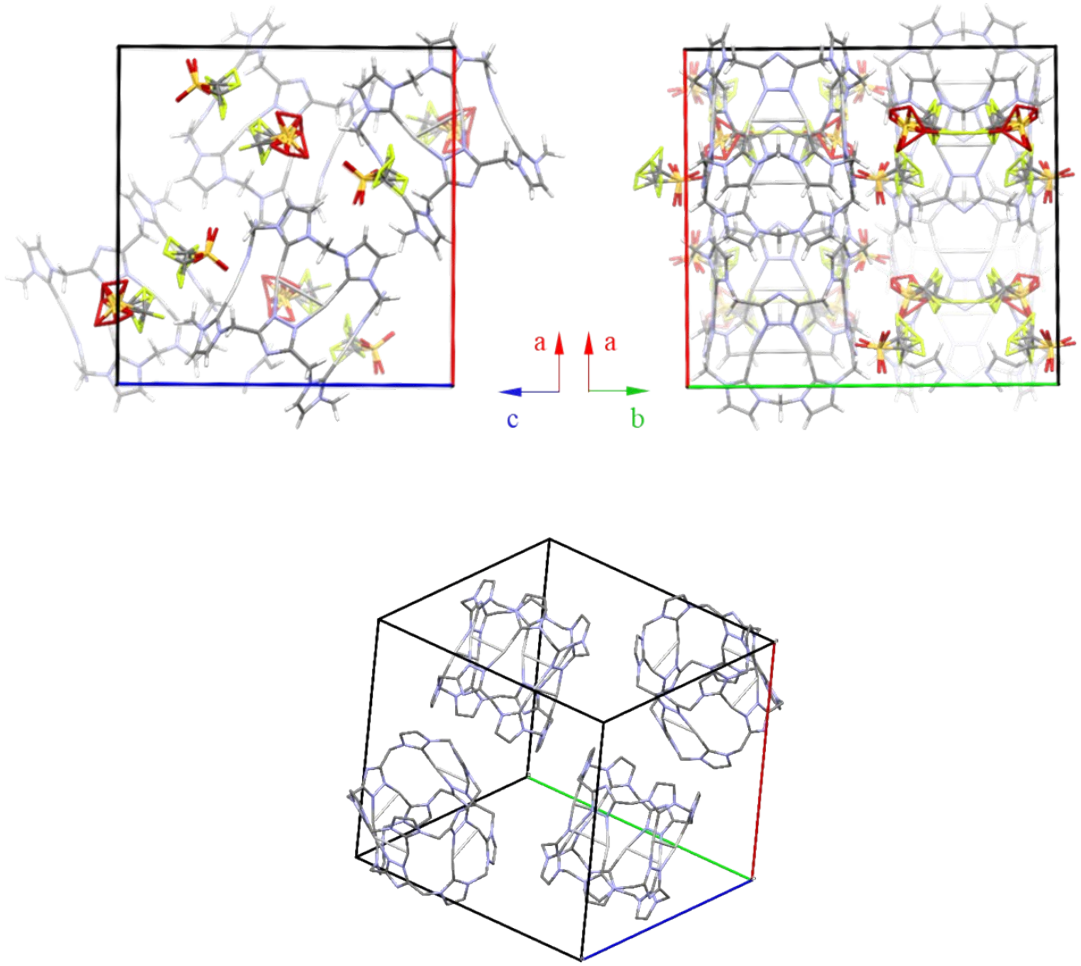

Figure S23. (Top) Solid-state packing of **[$Ag_8L^t_2$](OTf)$_4$** with all triflate anions being structurally disordered and (bottom) packing of the **[$Ag_8L^t_2$]$^{4+}$** cations.

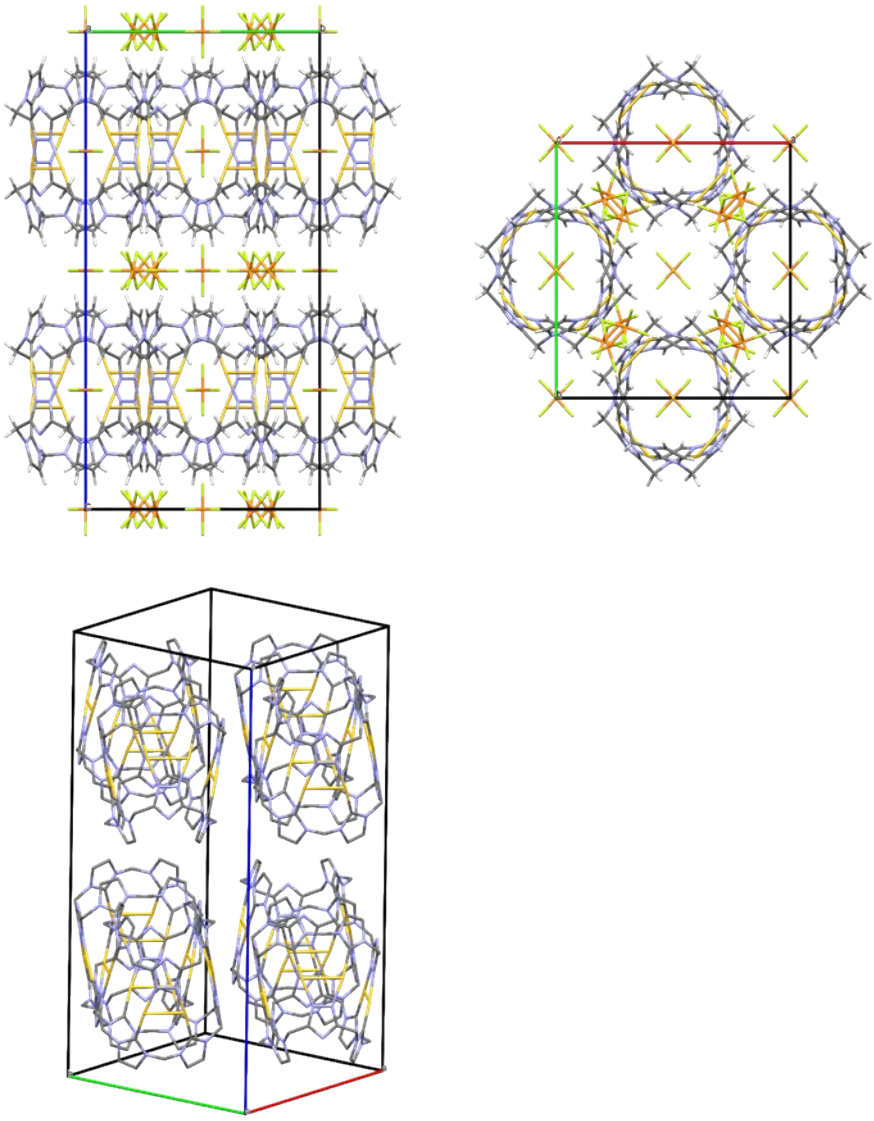

Figure S24. Packing of **[$Au_8L^t_2$](PF_6)$_4$** in the solid state: (top left) view along the crystallographic ***a***-axis; (top right) view along the crystallographic ***c***-axis; (bottom) packing of the cations (hydrogen atoms are omitted for clarity)

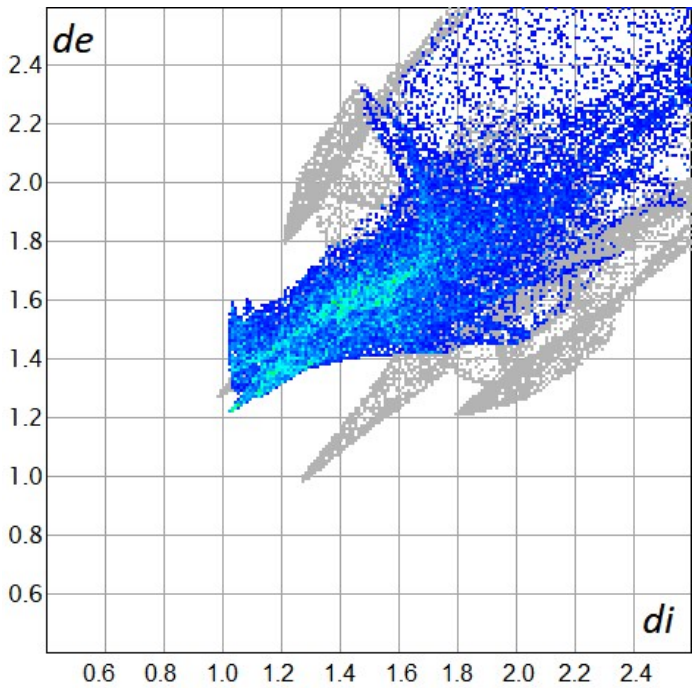

Figure S25. Hirshfeld surface analysis fingerprint plots of the P-F···H interactions in **[$Au_8L^t_2$](PF_6)$_4$** (54.8% of the total interactions).

13. References

1. K. Choi and A. D. Hamilton, Selective anion binding by a macrocycle with convergent hydrogen bonding functionality, *Journal of the American Chemical Society*, 2001, **123**, 2456-2457.
2. M. A. Hossain, J. M. Llinares, S. Mason, P. Morehouse, D. Powell and K. Bowman-James, Parallels in cation and anion coordination: a new class of cascade complexes, *Angewandte Chemie*, 2002, **114**, 2441-2444.
3. P. Kuzmič, Program DYNAFIT for the analysis of enzyme kinetic data: application to HIV proteinase, *Anal. Biochem.*, 1996, **237**, 260-273.
4. P. J. Altmann and A. Pöthig, Pillarplexes: A Metal–Organic Class of Supramolecular Hosts, *J. Am. Chem. Soc.*, 2016, **138**, 13171-13174.
5. F. Neese, Software update: the ORCA program system, version 4.0, *WIREs Computational Molecular Science*, 2018, **8**, e1327.
6. F. Neese, The ORCA program system, *WIREs Computational Molecular Science*, 2012, **2**, 73-78.
7. F. Neese, ORCA: an ab initio DFT and semiempirical SCF-MO package, *University of Bonn, Bonn, Germany*, 2007.
8. J. Perdew, S Burke and M Ernzerhof Phys, *Rev. Lett.*, 1996, **77**, 3865.
9. F. Weigend and R. Ahlrichs, Balanced basis sets of split valence, triple zeta valence and quadruple zeta valence quality for H to Rn: Design and assessment of accuracy, *Physical Chemistry Chemical Physics*, 2005, **7**, 3297-3305.
10. F. Weigend, Accurate Coulomb-fitting basis sets for H to Rn, *Physical chemistry chemical physics*, 2006, **8**, 1057-1065.
11. S. Grimme, S. Ehrlich and L. Goerigk, Effect of the damping function in dispersion corrected density functional theory, *Journal of computational chemistry*, 2011, **32**, 1456-1465.
12. S. Grimme, J. Antony, S. Ehrlich and H. Krieg, A consistent and accurate ab initio parametrization of density functional dispersion correction (DFT-D) for the 94 elements H-Pu, *The Journal of chemical physics*, 2010, **132**, 154104.
13. M. Bruker AXS Inc., Wasconsin, USA, unpublished work.
14. M. Bruker AXS Inc., Wasconsin, USA, unpublished work.
15. C. B. Hübschle, G. M. Sheldrick and B. Dittrich, ShelXle: a Qt graphical user interface for SHELXL, *Journal of applied crystallography*, 2011, **44**, 1281-1284.
16. G. Sheldrick, SHELXL-2014/7: program for the solution of crystal structures, *University of Göttingen, Göttingen, Germany*, 2014.
17. G. Sheldrick, SHELXL-97 (Release 97-2) University of Göttingen.*Journal*, 1998.
18. A. Wilson, ed. E. Prince, Kluwer, Dordrecht, The Netherlands, 1992, vol. C, ch. Mathematical, Physical and Chemical Tables, pp. 500-502, 219-222, 193-199.
19. A. L. Spek, PLATON SQUEEZE: a tool for the calculation of the disordered solvent contribution to the calculated structure factors, *Acta Crystallographica Section C: Structural Chemistry*, 2015, **71**, 9-18.
20. A. L. Spek, Structure validation in chemical crystallography, *Acta Crystallographica Section D: Biological Crystallography*, 2009, **65**, 148-155.
21. C. B. I. Macrae and J. Chisholm, A Edgington P. R McCabe P Pidcock E Rodriguez-Monge L Taylor R van de Streek J Wood P, *A J. Appl. Cryst*, 2008, **41**, 466.
22. B. Cordero, V. Gómez, A. E. Platero-Prats, M. Revés, J. Echeverría, E. Cremades, F. Barragán and S. Alvarez, Covalent radii revisited, *Dalton Transactions*, 2008, **21**, 2832-2838.